Accepted Manuscript

Low-Cycle Fatigue Characterization and Texture Induced Ratcheting Behaviour of Forged AZ80 Mg Alloys

A. Gryguc, S.B. Behravesh, S.K. Shaha, H. Jahed, M. Wells, B. Williams, X. Su

PII: S0142-1123(18)30254-8
DOI: https://doi.org/10.1016/j.ijfatigue.2018.06.028
Reference: JIJF 4732

To appear in: *International Journal of Fatigue*

Received Date: 1 February 2018
Revised Date: 15 June 2018
Accepted Date: 18 June 2018

Please cite this article as: Gryguc, A., Behravesh, S.B., Shaha, S.K., Jahed, H., Wells, M., Williams, B., Su, X., Low-Cycle Fatigue Characterization and Texture Induced Ratcheting Behaviour of Forged AZ80 Mg Alloys, *International Journal of Fatigue* (2018), doi: https://doi.org/10.1016/j.ijfatigue.2018.06.028

Low-Cycle Fatigue Characterization and Texture Induced Ratcheting Behaviour of Forged AZ80 Mg Alloys

A. Gryguc [1], S.B. Behravesh[1], S.K. Shaha[1], H. Jahed [1*], M. Wells [1], B. Williams[2], X. Su[3]

[1]Department of Mechanical & Mechatronics Engineering, University of Waterloo, 200 University Avenue West, Waterloo, ON N2L 3G1, Canada
[2]CanmetMATERIALS, Natural Resources Canada, 183 Longwood Road South, Hamilton, ON L8P 0A1, Canada
[3]Ford Research and Innovation Center, 2101 Village Road, Dearborn, MI 48124, USA

ABSTRACT

Stress-controlled uniaxial "push-pull" fatigue testing was conducted on as-received (cast and extruded) and closed-die cast-forged and extruded-forged AZ80 Mg alloy. The as-cast material possessed random texture and somewhat symmetric cyclic responses. The extruded and forged materials possessed sharp basal texture and asymmetric cyclic responses. All materials exhibited tension/compression asymmetry in their cyclic response to varying degrees, depending on the thermomechanical processing conditions. It was discovered that the style of closed-die forging being investigated had spatially varying properties with texture orientations which varied based on the local forging directions and intensities which were dependent on the starting texture as well as the thermomechanical history. Under fatigue testing, the materials all developed some form of mean strain, with the nature and magnitude of this mean strain being dependent on primarily its texture intensity and propensity to twin in either tension or compression reversals. The type of mean strain (tensile or compressive) depends upon both the orientation and intensity of the starting texture of material. The texture induced ratcheting and resulting mean strain evolution was most pronounced in the as-cast material and had a significant impact on the fatigue life. Following forging, the material exhibited an increase in fatigue life of anywhere from 2 to 15 times for the cast then forged material and more modest yet still significant 8 times longer at stress amplitudes around 140 MPa for the extruded then forged material. The extruded forged material exhibited similar fatigue lives to that of the base material at stress amplitudes which approached the yield strength. The nature of the mean stress development and degree of fatigue life improvement depended on the processing conditions and the type of base material (cast or extruded) utilized to create the forging. Two energy based models were utilized to predict the life of the forged material, and gave a reliable life prediction for a variety of material conditions that were investigated.

Keywords: Magnesium, Forging, Fatigue Characterization, Ratcheting, Texture.

1. Introduction

There has been a strong motivation to increase fuel efficiency and decrease emissions in the automotive industry over the past several decades. Implementation of lightweight materials in structural applications are at the forefront of this effort, as this strategy can improve vehicle efficiency, longevity, and performance. Magnesium (Mg) and its alloys have significant promise in this area, with widespread applicability in fatigue-critical components, such as suspension control arms, since they are the lightest commercially available structural metal and their cyclic properties are similar to those of the heavier,

* Corresponding author: agryguc@uwaterloo.ca

more conventional materials used in industry [1]. The focus of the present study is to examine the effect that closed die forging has on the monotonic, stress controlled cyclic behaviour and texture induced ratcheting of AZ80 Mg.

Although there has been some limited work done on the fatigue behaviour of the AZ family of Mg alloys [2]–[10] virtually all of it is focused on cast, extruded or rolled varieties and not material processed by means of warm forging. Alongside this, many researchers have focused on the high temperature deformation behaviour of forged AZ80 [11]–[28] however little to no work had been done in the past on the characterization of forged Mg alloys. More recently, extensive work has been done thus far on the pioneering of characterizing forged Mg [29]–[35] especially its fatigue behaviour. He et al. [36] explored the influence on initial billet as well as die geometry (open-die vs. semi-closed) for a large AZ80 Mg component forged at 380°C. They found that with an open-die configuration over 32% of the final forging had an effective strain of less than 0.5 with large spatial variation in the strain indicating that a considerable part of the final component had not been sufficiently deformed to achieve the full benefit in material properties. However when utilizing a semi-closed die for the same forging only 3% of the final component had an effective strain of less than 0.5 indicating that virtually all of the forging had been evenly and sufficiently deformed. Furthermore, they stated that the semi-closed die forgings had an even and refined microstructure with virtually no material anisotropy in tensile properties between the longitudinal and transverse directions within the forging. Wang et al. [37] investigated the microstructure and mechanical properties of cast-homogenized AZ80 that was open-die forged at 8 mm/sec at temperatures ranging from 200-400°C and equivalent strains of 80-265%. They found that with increasing levels of equivalent strain the forged material exhibited higher tensile strengths and ductility, while the more ductile properties favoring higher forging temperatures. They also found that the maximum tensile strength was achieved when forged at 250°C at a maximum induced strain of 265%. Previous work by Gryguc et al. [33] investigated the monotonic and cyclic behaviour of as cast and cast-forged AZ80 Mg in a simple open die configuration at 350°C and 450°C forging temperatures and rates ranging from 0.6 – 6 mm/sec. It was found that the mechanical properties are much more sensitive to forging temperature than forging rate and that even with an open die configuration the final component had been sufficiently deformed to have almost fully recrystallized and not exhibit any similarities to the base materials cast-dendritic microstructure. Furthermore, it was found that once forged, the material developed appreciable texture which was very different from that of the randomized as-cast materials texture, and this texture development influenced the mechanical response in both static and fatigue testing.

In this study, the effect of base material condition on the tensile/fatigue behaviour of AZ80 was examined in detail in a closed die forging with highly three-dimensional material flow. Furthermore, the spatial variation of mechanical properties throughout the forging was investigated and a texture and microstructural link to these properties were established. Furthermore, a correlation between the materials local texture and the mean strain development in the cyclic response is discussed. Results from a fully-reversed stress-controlled fatigue test in the low-cycle regime are presented. Energy-based fatigue models were used predict the fatigue life of cast, extruded, cast-forged and extruded-forged AZ80 Mg, and their accuracy was also examined.

2. Material and Experiments

The material used in this investigation was commercially-available AZ80 Mg alloy in the forms of cast and extrusion (8.0 ±0.2% aluminum content, with other elements composition as per ASTM B91-12 standard). The material was received from Magnesium Elektron North America Inc. in the form of as-cast and extruded billets in the as-fabricated condition. The dimension of the as-cast billet are 300 mm in diameter and a length of 500 mm, while the extruded billet was a diameter of 63.5 mm and a length of 1000 mm. The forging of the as-cast and extruded material was conducted at CanmetMATERIALS (Hamilton, Canada) using the billets having dimension of ⌀ 63.5 mm, 65-mm long. The as-cast billets

were machined from the 300-mm diameter AZ80 casting, and the as-extruded billets were simply cut to length prior to forging. All forgings were carried out on a 500-ton hydraulic press with a profiled upper and lower die with an I-beam shaped internal cavity. A typical forged part produced by these dies is shown in Figure 1. The billet and tooling were heated separately to 375°C for sufficient time to allow any thermal gradients to decay. The orientation of the billet to the press was such that the radial direction was along the direction of the press stroke (i.e. the direction of forging was parallel to the radial direction of the billet). Forging was carried out in a single step at a displacement rate of 20 mm/sec. Figure 1 illustrates a forgings conducted at 375°C and 20 mm/sec. The forging direction (FD) is normal to the web face, with the longitudinal direction (LD) being parallel to the axis of the flanges and transverse direction (TD) being perpendicular to flange axis. In the image (b) a red rectangle denotes the interface between the forged component and the flash region. Everything internal to the denoted rectangle is considered a part of the forging and everything external is considered "flash" or scrap material.

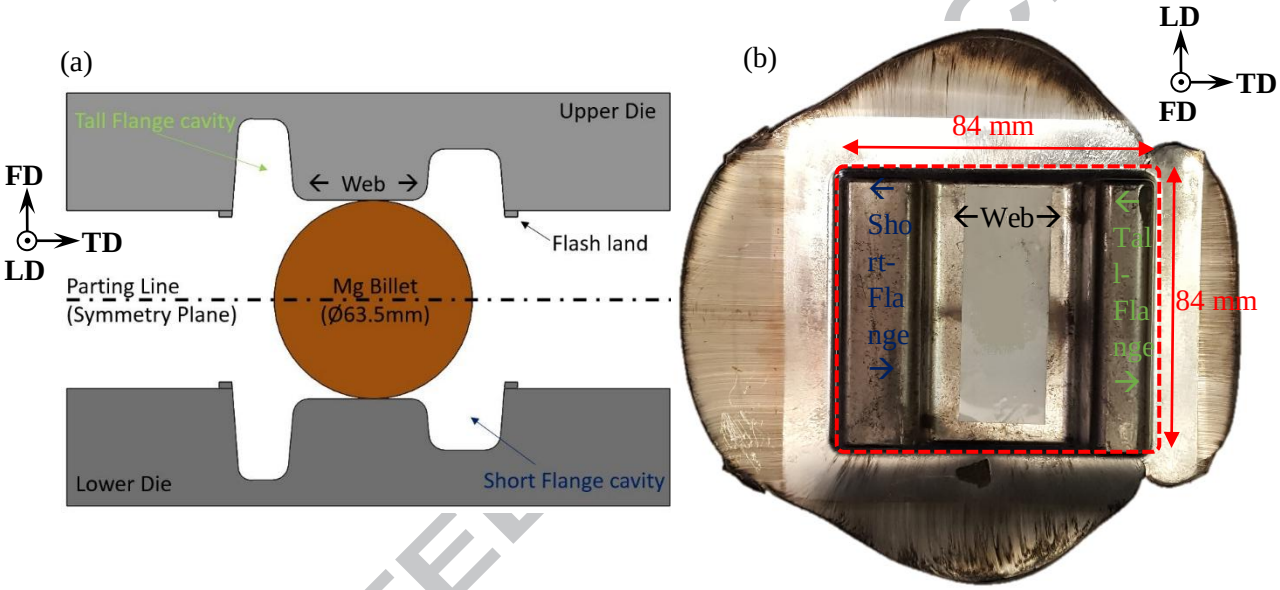

Figure 1 – (a) schematic of AZ80 Mg closed die forgings with asymmetric I-beam cross section conducted at (b) 375°C and 20 mm/sec ram speed prior to trimming off the flash extruded then forged.

The metallographic samples were prepared following the standard metallographic techniques outlined in ASTM E3-11 with acetic-picral etchant similar to that used by Roostaei et al. [38]. The microstructure was observed using a light optical microscope (LOM) and a scanning electron microscope (SEM), coupled with energy-dispersive X-ray spectroscopy (EDS). The average grain intercept method is used to quantify the grain size according to ASTM E112-12.

The texture measurements were performed on polished samples using a Bruker D8-Discover equipped with a VÅNTEC-500 area detector, with a radius of 135 mm and using Cu-Kα radiation at 40kV and 40 mA. During the measurement, the incident beam and the detector were placed at a fixed 2θ angle of 40°. The collimator size was 1.0 mm. The sample was mounted on the motorized stage, which was oscillated at an amplitude of 1.5 and 2.5 mm, and a speed of 3.5 mm s^{-1} and 5.5 mm s^{-1} for the *X* and *Y* axis, respectively. The samples were tilted between 0 and 75°, with a step of 15° considered as the Ψ-scan, while the sample rotation, known as Φ-scan, was between 0 and 360°, with a step size of 5°. The sample was scanned for 20 s at each orientation. The Debye–Scherrer diffraction rings were collected using the area detector in a 2-D diffraction image. Then, the incomplete pole figures for the {0002}, $\{10\bar{1}0\}$, $\{10\bar{1}1\}$, and $\{1\bar{1}02\}$ planes were extracted from the diffraction rings. The complete pole figures were then calculated using the DIFFRAC.Suite: Texture software.

Tensile test samples with geometries according to Roostaei et al. [38] and a 4 mm thickness were extracted from the as-received billet and closed die forged samples. The as-cast samples were extracted from a location within the billet where the middle of the gauge section was at 70% of the billets radius. The extruded samples were machined along the extrusion direction and from a location where the middle of the gauge section was at 50% of the billets radius. There were 15 test samples that were extracted from 15 different locations throughout the closed die forging (all having their axis parallel with the LD direction), as shown in Figure 2 (d). These samples were later utilized for quasi-static and cyclic testing. The quasi-static tensile tests were performed according to ASTM standard E8/E8M-15a using an MTS 810 Servo-Hydraulic test machine operating in displacement control mode with a displacement rate of 1 mm/min. Strain measurement was accomplished using a GOM ARAMIS 3D 5MP DIC system. The average strain rate within the gauge section of measurement was 1.4E−3 sec^{-1}.

The fatigue tests were performed as per ASTM E466-15 in an ambient environment using an MTS 810 Servo-Hydraulic test machine operating in stress control mode at a frequency range of 0.1 Hz to 30 Hz depending on the stress amplitude to maintain an approximately consistent loading rate between all tests. The strain was measured throughout the first 10,000 cycles using an MTS 632.26 extensometer with an 8-mm gauge and travel of ± 1.2-mm until stabilization of the cyclic hysteresis loop was achieved. The tests were conducted at a zero mean stress (i.e., $R_L = -1$, fully reversed stress cycle) and stress amplitudes of between 140 MPa and 190 MPa. The failure criteria for the tests were considered to be final rupture of the specimen gauge section. The fracture surfaces after tensile and fatigue tests were examined using SEM techniques (FEI Quanta FEG 250 ESEM with EDX).

3. Results and Discussion

3.1 Microstructure and Texture

Table 1 highlights the relationship between microstructural, monotonic and cyclic properties of as-received (as-cast and as extruded) and forged (CF: Cast Forged and EF: Extruded Forged) AZ80. The conditions for forging were the same for both CF and EF at a forging temperature of 375°C and 20 mm/sec of ram speed. The grain size is quite uniform throughout various locations of the as-received billets; however, there is notable spatial variation in the microstructure throughout the cross-section of the forgings. As such, the grain size and tensile properties are presented at two different locations within the forging, location 1 which is considered to be the top of the tall flange region of the forging and location 8 which is considered the web region which connects the two flanges. Although beyond the scope of this study, 3D forging simulation revealed that in the final step of forging, the web region was the location that incurred the most amount of equivalent plastic strain, decaying as moving up the height of the flanges [39]. This is due to the complex material flow, which is expected, in a closed die forging of this cross section as well as the fact that the web region has the most amount of height compression relative to the initial billet diameter. Gryguc et al. [33] characterized the microstructure of as-cast AZ80 to consist of primarily α-phase, in which aluminium-rich β-phase ($Mg_{17}Al_{12}$) is precipitated along the grain boundaries. This agrees with the microstructure of as-cast AZ80 observed by Nový et al. [40], the grain morphology of which was very similar to that which is presented in this study, while the average grain size (80–140 μm) was slightly more refined than that observed in this study. Finally, the Rockwell hardness presented in Table 1 is an average across the entire cross-section of the forging, however, as one might expect it also spatially varies to a moderate degree as shown by the contour plots in figures Figure 2 (d) and Figure 3 (d). In these contour plots, areas in red represent the regions with the highest superficial hardness, and it can be seen that the web region (location 8-10) shows the highest indicated hardness in the cast-forged material. In the extruded-forged material, the spatial variation of hardness is much lower, and the selected scale exaggerates any non-uniformities, however it can be observed that the lowest hardness is

consistently seen at the top and bottom corners of each flange. Figure 2 shows a summary of the microstructure, texture and superficial hardness variation for the cast-forged I-beam forging with Figure 2 (a) (b) and (f) show the XRD pole figures for the basal and prismatic planes for 3 different locations within the forging (the tall flange (Location 1), short flange (Location 15) and web (Location 8)). Furthermore, Figure 2 (c) and (e) illustrate the microstructure for two locations in the forging, the tall flange, and web, respectively. It can be observed that the basal pole figure shows somewhat of a randomized pattern in both of the flange locations, however in the web region evidence of a less random and more intense texture can be observed by the pattern in the basal pole figure in Figure 2 (f). This somewhat randomized texture, which remains from the parent as-cast material, can be attributed to non-fully recrystallized grain structure in certain regions of the forging as can be seen in both LOM images (c and e) where a somewhat coarse grain structure is still evident with little evidence of partial dynamic recrystallization (DRX) as noted in Figure 2 (c) and (e).

Table 1- The relationship between microstructural, superficial hardness, and monotonic properties of as-cast, as-extruded and cast-forged (CF) and extruded-forged (EF) AZ80 Mg alloy. Tensile properties are presented first, followed by compressive properties in parenthesis, where available.

Material	Rate (mm/min)	Temp (°C)	Location in Billet	Grain size (μm)	HR-30T	σ_{YS} (MPa)	ε_{Fail} (%)	σ_{ULT} (MPa)
As-Cast	-	-	70% of radius	178.9±67	27.2	92.8 (93.8)	7.4 (15.3)	220.9 (318.2)
As-Ext	-		50% of radius	18.0±0.7	35.4	195.4	11.3	341.1 (412.1)
CF	20	375	Tall flange #1	37.7±5.3	19.9	110.7	7.2	239.8
			Web #8	23.2±3.9	26.9	175.0	14.1	312.1
EF			Tall flange #1	17.5±1.6	30.5	226.8	17.5	351.1
			Web #8	15.2±1.0	32.1	219.2	20.5	341.3

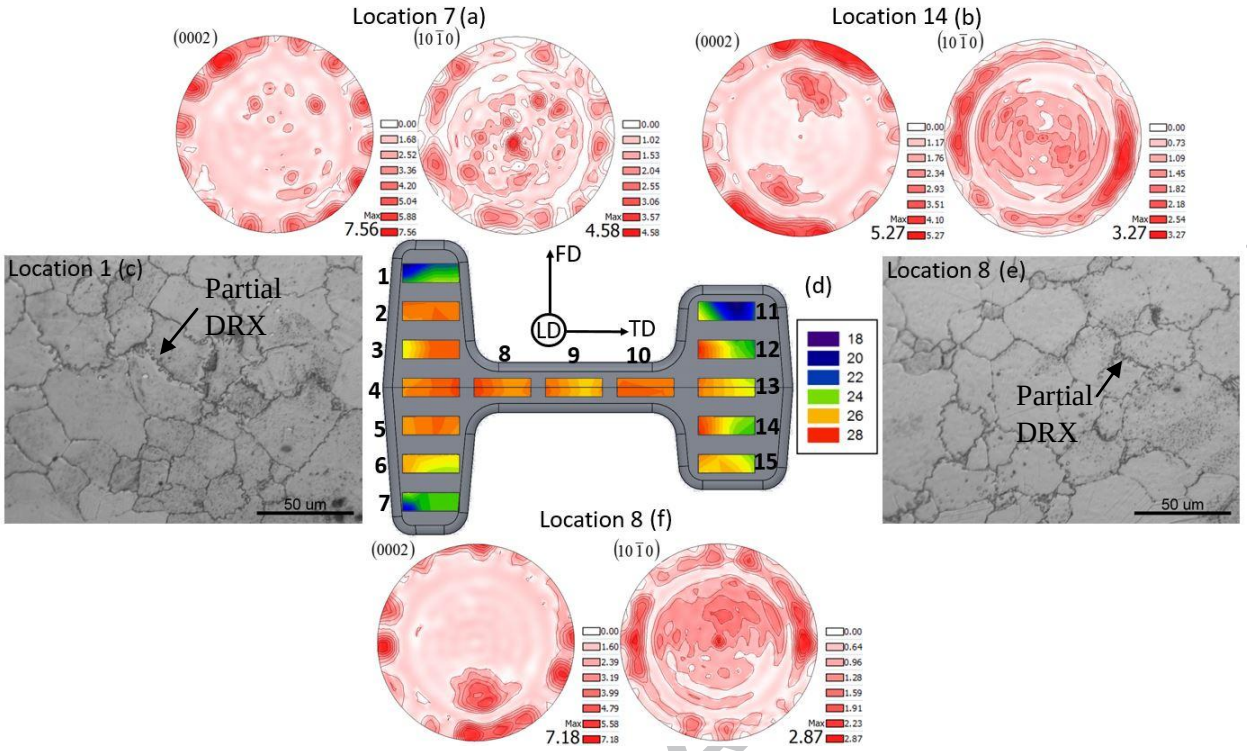

Figure 2 – Microstructural characterization of Cast AZ80 forged at 375°C and 20 mm/sec. Basal and prismatic pole figures are presented in locations 7 (a), location 15 (b), and location 8 (f) of the forging. Figure (c) and (e) show LOM images of locations 1 and 8, respectively within the forging (view in the longitudinal direction). Figure (d) denotes the spatial variation of superficial hardness (30T) in the direction normal to the cross-section of the forging. FD denotes forging direction, TD: transverse direction, and LD: longitudinal direction.

Figure 3 presents the same type of information in an identical format to that of Figure 2 however for the extruded and forged component. It is well known that AZ80 Mg has significant texture when processed by method of extrusion [32], and that forging reorients the texture in such a way that the c-axises of the HCP crystal structure are parallel with the local forging direction [30]–[33], [41], [42]. Thus, it can be expected that not only will the extruded-forged component have an intense texture, but this texture will vary throughout the cross-section of the forging and be a function of the local forging direction and the complex three-dimensional material flow. This expectation is supported by the basal and prismatic pole figures presented in Figure 3 (a) (b) and (f), with relative intensities that are much higher than those of the cast-forged variety and spatially varying intensity peaks that align themselves to the local forging direction. Finally, the microstructural images in Figure 3 (c) and (e) show a much more refined microstructure relative to that of the cast-forged I-beam with the web region (location 8) having more refined structure (compared to location 1), which supports the fact that this region of the forging had the higher superficial hardness Figure 3 (d) and ductility as shown in Table 1.

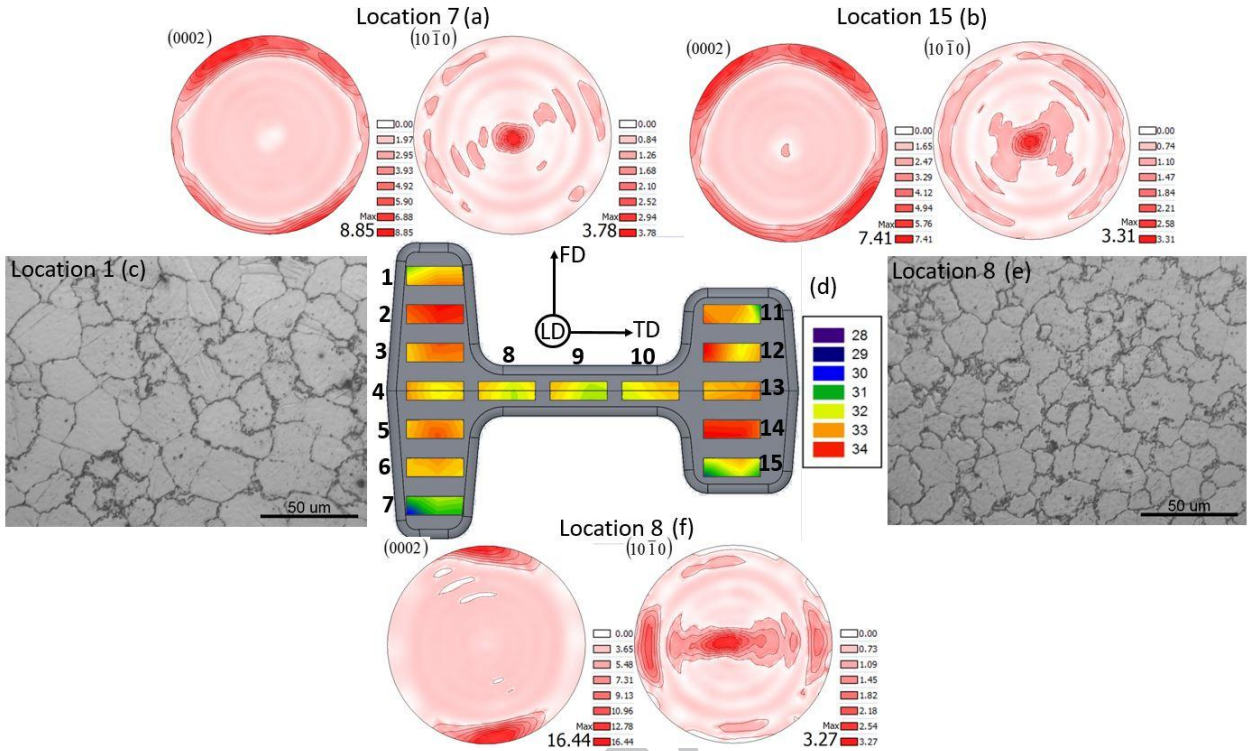

Figure 3 - Microstructural characterization of AZ80 extrusion forged at 375°C and 20 mm/sec. Basal and prismatic pole figures are presented in locations 7 (a), location 15 (b) and location 8 (f) of the forging. Figure (c) and (e) show LOM images of locations 1 and 8, respectively within the forging (view in the longitudinal direction). Figure (d) denotes the spatial variation of superficial hardness (30T) in the direction normal to the cross-section of the forging. FD denotes forging direction, TD: transverse direction, and LD: longitudinal direction.

3.2 Monotonic and Cyclic

Figure 4 shows the engineering stress vs. engineering strain tensile monotonic response for the as received and forged materials at two different locations within the forging. It can be observed that in both the CF and EF forgings, the web region has the highest ductility. Furthermore, the EF material has higher strength and ductility relative to the CF material, and a large increase in ductility once forged is apparent relative to the parent as-extruded material. The qualitative correlation can be made that in regions with higher equivalent strain imposed by forging (such as in the web region) possess a higher superficial hardness and superior strength and ductility to other regions of the forging, especially in the cast-forged material. For the extruded forged material, the yield and ultimate strength are fairly similar to the parent material, however, the ductility is much improved. Future work in this study is concentrating on lower temperature forgings, and it is expected that at temperatures ranging from 250-275°C a significant increase in strength can be achieved relative to the parent as-extruded material.

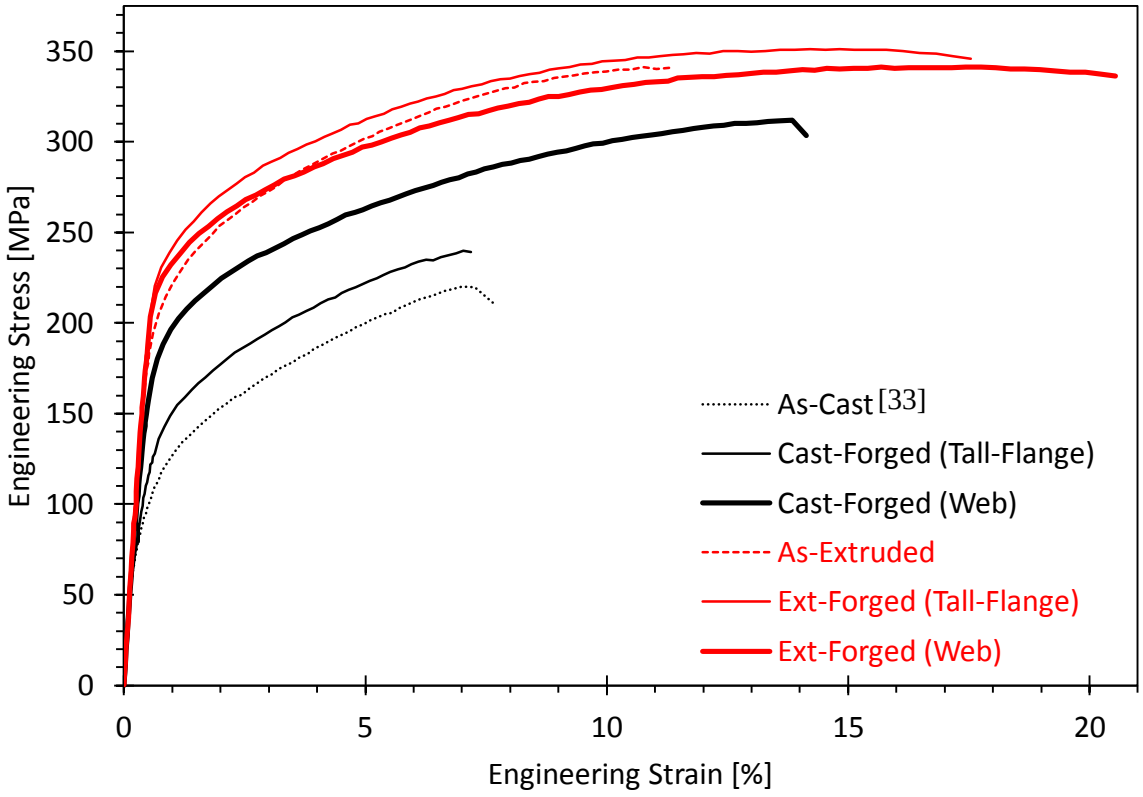

Figure 4 - Tensile monotonic engineering stress-strain curves for as-received materials as well as cast-forged and extruded forged conditions in two different locations within the forging. The tall-flange corresponds with location 1 and the web corresponds to location 8.

Figure 5 illustrates the cyclic stress-strain hysteresis response for the as-cast and cast-forged materials obtained during fully reversed ($R_L = -1$) stress controlled testing at a stress amplitude of 190 MPa. The first cycle (reversals 2 and 3) is shown as symbols whereas the stabilized cycle is shown as solid lines. Figure 6 illustrates the same information for as-extruded and extruded-forged materials. For the CF and EF materials the locations within each forging where the cyclic response is presented is denoted in each caption. It can be observed that in the as-cast material the first cycle is characterized by a very large amount of plastic strain energy (or area enveloped by the hysteresis loop) and a large evolution in mean strain over the course of the first cycle (as can be seen by the disjointed tensile peaks for the first cycle hysteresis loop). This response can be attributed to the weak extension twinning in first tensile reversal which results in over 4% strain at 190 MPa. Although the as-cast material possesses a random texture, the weak twinning is caused by some proportion of grains being favorably oriented for extension twinning during the first reversal. Then, in the 2nd and 3rd reversals, the strain amplitude decreases as the material has already begun to accumulate both twin and dislocation density and cyclically harden. The twin density is not only a function of a number of cycles, it is also a function of the state of stress within each cycle as the twinning process is not fully reversible resulting in residual twin accumulation [33], [43]. Thus, the positive mean strain begins to decrease cycle by cycle as the material hardens, this eventually leading to the stabilized response where the hysteresis loop is symmetric in compression and tension and exhibits ~0.5% of tensile mean strain. Important to note is the shape of both the ascending and descending reversals in the as-cast material is only slightly sigmoidal as the twinning and detwinning process are diffuse, and only occur to grains which possess favourable orientation within the materials randomized

texture. The cast-forged material, however, exhibits a response with much fewer plastic strain energy, due to the fact that the strain required to achieve 190 MPa in tension is much lower in the cast-forged material as can be observed in Figure 4. Furthermore, as presented in previous studies [33], there is pronounced yield asymmetry in the cast-forged AZ80, more specifically the compressive yield is lower than the tensile, which manifests itself as a large strain range required to achieve 190 MPa in compression in the 2nd reversal. This results in a significant compressive mean strain in first cycle which continues as the material cyclically hardens to the stabilized response of the cast-forged material.) It can be seen in the cast-forged materials downward reversal of the first cycle that the reverse yielding is very sharp indicative of prominent compressive twinning due to the intense texture and associated large proportion of grains with a favourable orientation for extension twinning in compression. This sharp reverse yielding is characteristic of a large proportion of grains which twin to accommodate the deformation, Following this, a very sigmoidal ascending reversal occurs due to the vigorous detwinning which occurs [33]. As the cast-forged material cyclically hardens the plastic strain energy decreases as can be observed by the comparatively lower enveloped area by the stabilized hysteresis loop.

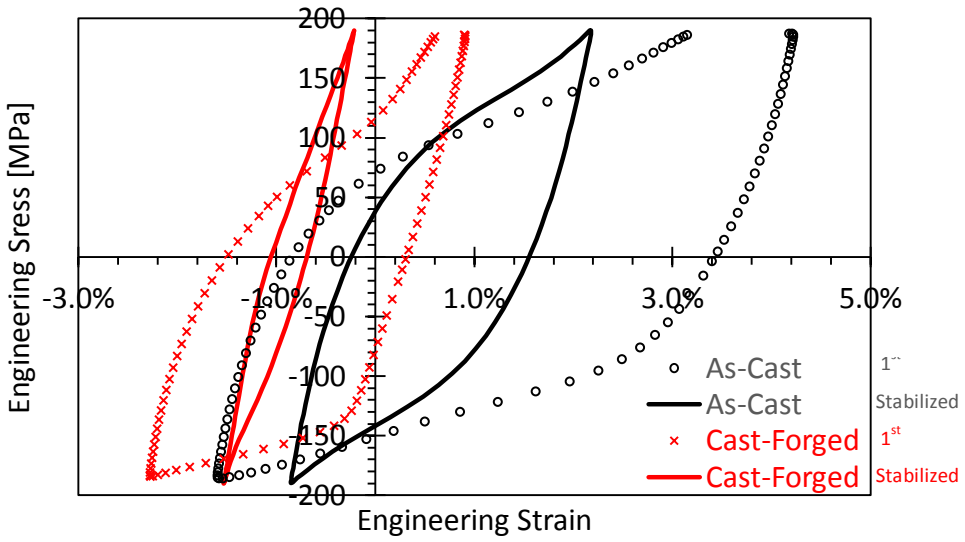

Figure 5 - The axial cyclic behaviour of as-cast and cast-forged AZ80 at a fully reversed stress amplitude of 190 MPa. Forged samples were taken from location 3 in tall-rib

Figure 6 depicts the hysteresis loops for the first cycle and the stabilized cycle for the extruded and extruded-forged material for a stress amplitude of 190 MPa. Due to the higher strengths of the extruded and EF materials (relative to the as-cast and CF varieties), in general, the plastic strain energy is always less for an equivalent stress amplitude. Both the as-extruded and EF materials display a similar first cycle response to that of the CF material, characterized by a very sharp reverse yielding due to extension twinning in compression followed by a vigorous detwinning process in the ascending reversal. Here the EF material has a much more pronounced reverse yielding in the descending reversal (relative to the extruded response). As the hysteresis loop presented here is for a sample taken from a web location, which possesses very intense texture. This intense texture is due to a dominant local forging direction with the vast majority of grains having a high propensity to exhibit extension twinning in compression due to their c-axis orientation being normal to the direction of loading. Important to note is the fact that the material with random texture (as-cast AZ80) has a positive mean strain with a very dynamic mean strain evolution whereas a material with appreciable texture (CF, as-extruded, and EF AZ80) has a negative mean strain.

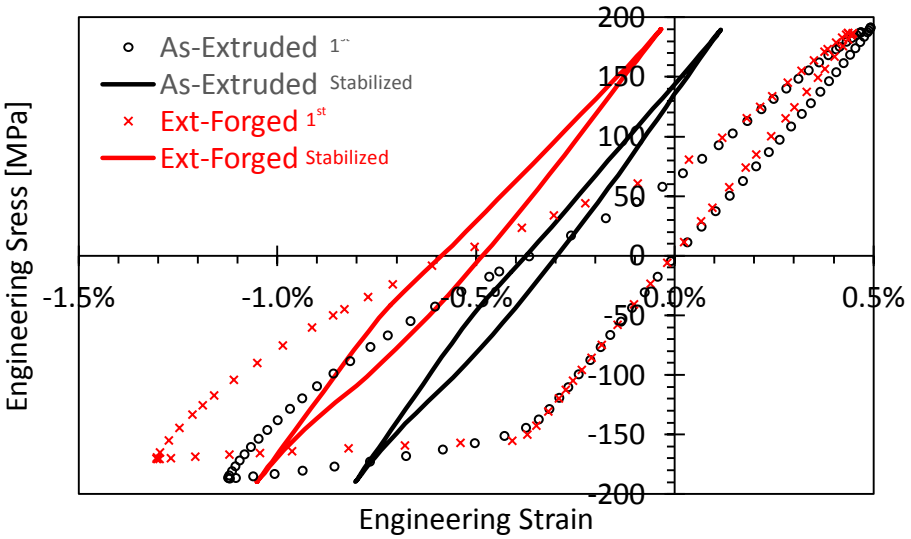

Figure 6 – The axial cyclic behaviour of as-extruded and extruded-forged AZ80 at a fully reversed stress amplitude of 180 MPa. Forged samples were taken from location 10 in the web.

Figure 7 illustrates the evolution of mean strain amplitude over the course of the cyclic testing. It can be seen that material with random texture (as-cast) will have diffuse extension twinning in the first reversal resulting in a large positive mean strain amplitude which decays as the material cyclically strain hardens. In contrast to this, all materials which possess appreciable texture (which have the c-axis oriented in a direction which is normal to the loading direction, such as the CF, extruded and EF samples), do not twin in the first reversal (as it is suppressed due to unfavourable grain orientation). That is, until the second cycle where they twin aggressively, resulting in a negative mean strain being developed. Since this detwinning process is more reversible in the significantly textured materials [43], the evolution of the mean strain is not as dynamic as the as-cast material despite the fact that they also cyclically strain harden. Important to note that the phenomenon of ratcheting (or accumulation of mean strain with accumulated cycles) is a direct artifact of the nature of as-cast Mg (or more generally, many randomized texture Mg alloys) to exhibit kinematic hardening during stress controlled cyclic testing. This ratcheting behaviour results in a dynamic evolution of mean strain where the hysteresis loop evolves in such a way

that the mean strain changes with accumulated cycles.

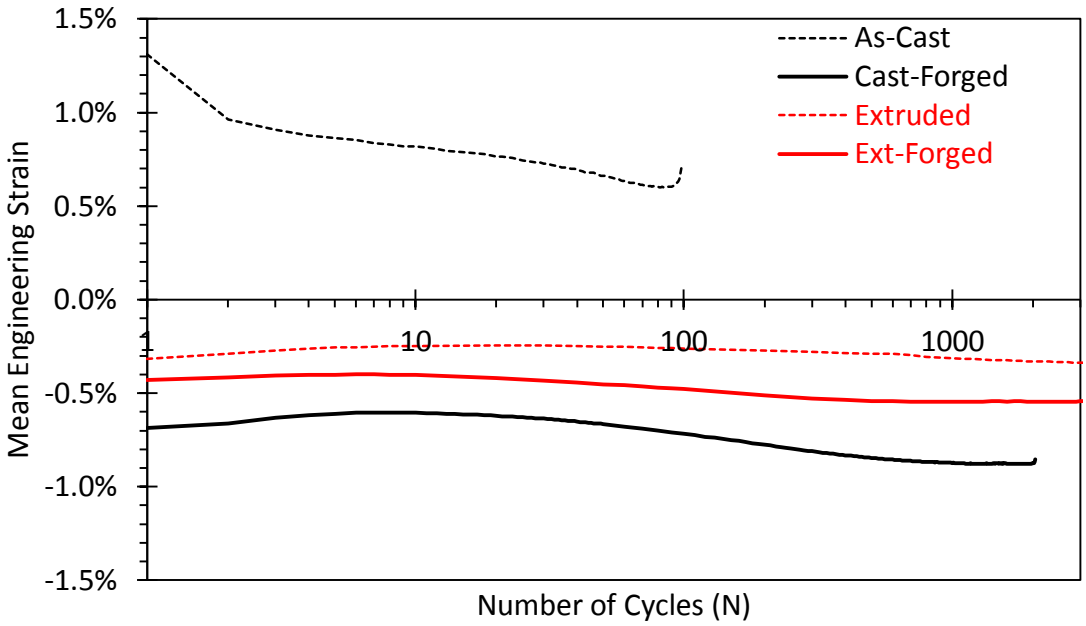

Figure 7 – Mean engineering strain response during stress-controlled cyclic testing for both as-received material as well as cast-forged and extruded-forged. Cast-forged response is shown for location 3 and extruded-forged for location number 10 within the web.

3.3 Fatigue Life

S-N data for all four material conditions have been presented in Figure 8. Axial strain was recorded only during a subset of all of these tests in order to capture the cyclic response and to gather the necessary data to check the applicability of existing energy-based life prediction models. It can be seen that there is a large improvement in the as-received materials fatigue performance once forged, with a larger improvement coming in the low-cycle regime for the CF material (as there is a large improvement in strength once the coarse cast microstructure is refined via forging). Contrasting to this, the significant improvement in fatigue performance is seen in the high-cycle regime for the EF material (as the ductility of the materials improves dramatically once forged). For LCF fatigue, the role that the elevated yield strength of the cast-forged material is the dominant factor in the improvement in fatigue performance relative to the as-cast material. However, for the mid-cycle fatigue and HCF, the response is virtually purely elastic and the effects of defect driven fatigue failures become more significant. In general, the extruded and extruded-forged materials have superior fatigue performance to the cast and cast-forged varieties which is to be expected.

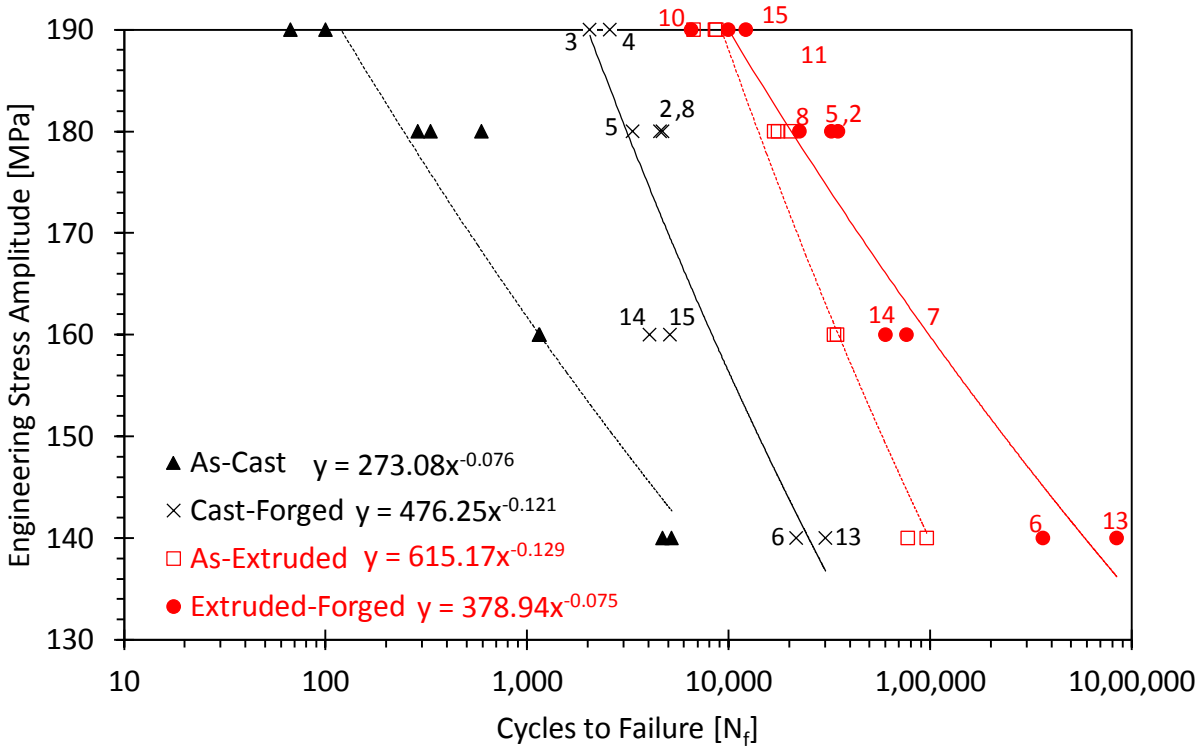

Figure 8 - S-N curves for as-cast and cast-forged (black) as well as as-extruded and extruded-forged (red) AZ80 Mg. Samples were taken from a variety of different locations throughout forging, location within forged billet denoted next to datapoint.

3.4 Fracture Mechanisms

Figure 9 illustrates the fracture surface for the cast-forged and extruded-forged material. Both surfaces are from samples at stress amplitudes of 190 MPa, which fractured at 2403 cycles and 6517 cycles respectively. The cast-forged surface is from a sample extracted from location 3 in the forged billet and the extruded forged was extracted from location 10 since both these locations have a comparable superficial hardness as indicated by previous Figure 2d and Figure 3d. The cast-forged surface, Figure 9 (a)(c)(e) exhibits multiple fatigue crack initiations (FCI's) primarily from the surface or just beneath as well as a number of large secondary cracks which progress to the interior of the sample similar to that found by Chen et al. [44]. In contrast to this, the extruded-forged fracture surface, Figure 9 (b)(d)(f), exhibits only one prominent FCI again originating virtually at the surface with no major secondary cracks. Based on EDX analysis of the FCI site, it can be determined that the cast-forged sample had several of its cracks initiate at brittle β-$Mg_{17}Al_{12}$ intergranular precipitates which were located at the surface and could be either granular or lamellar in their morphology similar to those found in other investigations [37], [45]–[47]. The granular shape of the β-phase agrees well with observations made by Wang et al [37] who found the divorced eutectic β-phase to be distributed along the α-phase grain boundaries in the as-cast state, but following hot compression, this eutectic network was broken up into both granular and lamellar shapes. In contrast to this, the single FCI in the extruded-forged condition had a few particles of Al_8Mn_5 compound that were located about 40 µm subsurface. Matrix debonding from these brittle particles appears to be the cause of crack initiation based on its proximity to the FCI and the intergranular faceted morphology of the fracture surface surrounding these granular particles emphasizing the brittle nature of that particular matrix/particle interface. Cai et al. [48] highlight the presences of this brittle compound

distributed in the grain interiors and boundaries of extruded AZ80, and the microstructure of their extruded material is very similar to that which was investigated in this study.

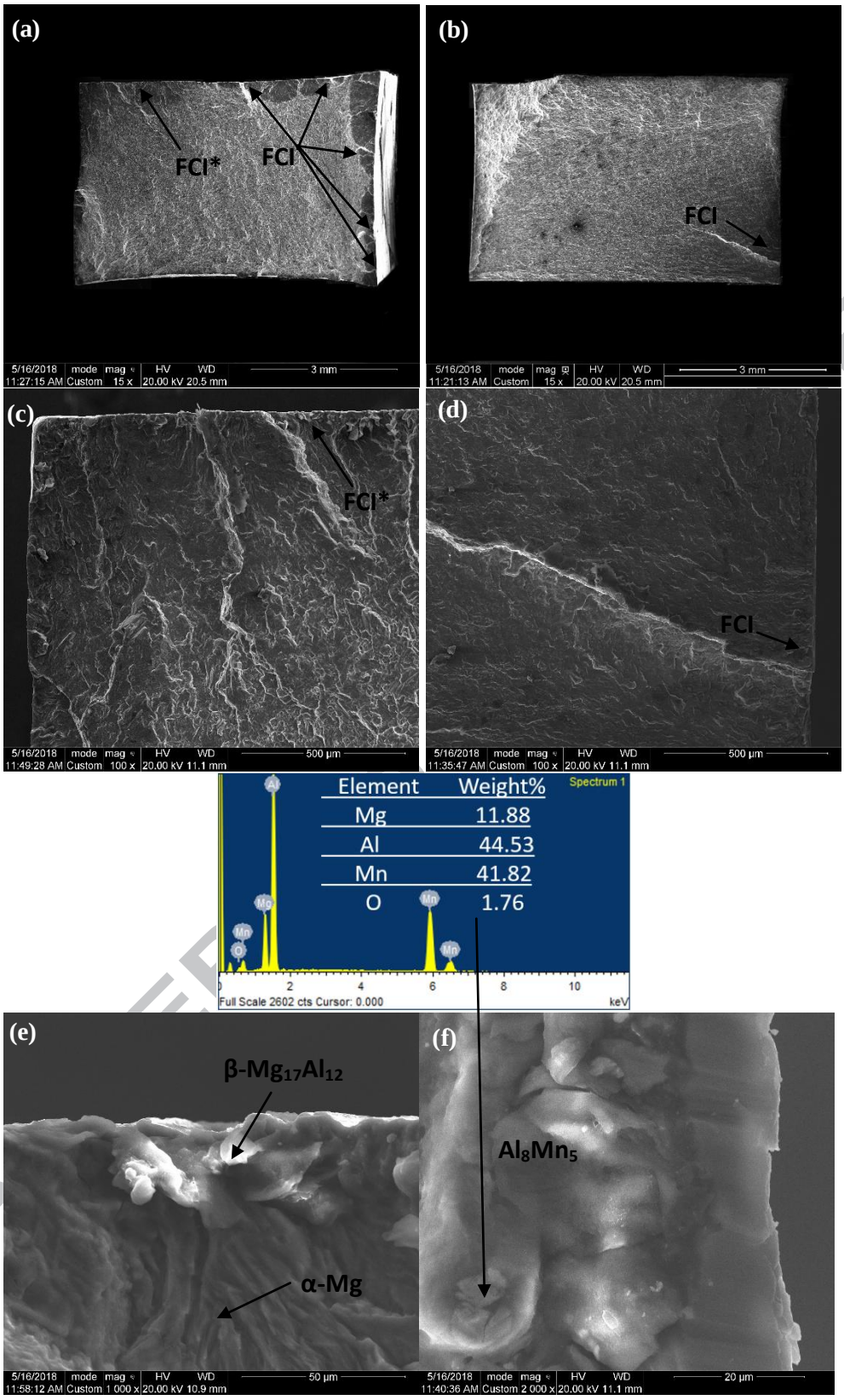

Figure 9 – Final fracture surfaces of the (a) cast-forged (b) and extruded-forged conditions for samples tested under stress control at 190 MPa. (a)(c)(e) are a cast-forged sample (b)(d)(f) are an extruded forged sample. FCI denotes fatigue crack location.

3.5 Fatigue Life Modelling

To quantitatively compare the damage incurred during cyclic loading in wrought Mg, numerous fatigue damage parameters, including stress-, strain-, and energy-based parameters have been proposed [42], [49]. Depending on the form of AZ80 being investigated the material response may vary between vigorous cyclic hardening [50], or even cyclic softening [51]. While successful attempts have been made to the model fatigue life of Mg alloys using stress-based damage model (e.g., [52] for hot-rolled AZ31B), in general, stress-based fatigue models are not ideal as they cannot accurately capture fatigue damage inflicted under these cyclic loading conditions. The objective of the following study is to investigate the suitability and accuracy of existing energy-based models at predicting the fatigue life of as-received and forged AZ80 material. The required material constants (model input parameters) were generated for each material condition according to the approach utilized in previous works [53], [54]. The energy-based two parameter model similar to Ellyin et al. [55] and Jahed-Varvani model [56] is examined here.

Energy-based fatigue damage models have been used by many researchers for modeling the fatigue life of Mg alloys, e.g., Park et al. [5], [57] in rolled AZ31, Xiong et al. [50] for rolled AZ80, for many different Mg alloys and conditions, and Albinmousa et al. [54], [58] for extruded AZ31 under multiaxial loading to predict the fatigue life of wrought Mg alloys. In this study, the JV model [56] is utilized to predict the life of the as-received material. Recent work [33] has been done utilizing this model to predict the fatigue life of as-cast and cast-forged open-die forged AZ80 Mg with good reliability. However, to predict the fatigue life of the closed-die forged material, the two-parameter energy based model was utilized, as the data presented here is from stress-controlled testing and is not adequate for generating the requisite material constants for the JV model. A comparison of the predicted fatigue life for both models is also discussed for the as-received material. The details of these models and their application to predict the fatigue life of wrought Mg alloys are described in studies by Roostaei et al. [59] and Jahed et al [54] for the JV and two parameter model respectively.

For the JV model, the energy-based parameters for cast AZ80 Mg found by Gryguc et al. [33] in a previous study are presented in Table 2. The fatigue life of the cast material was predicted for both the strain controlled test results presented in the previous study, as well as the stress-controlled stress results presented in this current study. Similarly, the fatigue life for the extruded material was also predicted. For the closed die forged material, a simple two parameter energy based model was used to correlate fatigue damage and predicted lives according to the relation:

$$\Delta W_t = C{N_f}^m \quad (1)$$

Where ΔW_t, is the total strain energy density as defined by the plastic and elastic components and C and m are fitting constants (not to be confused with the fatigue toughness exponent 'C', utilized in the JV model). In general uniaxial loading, the total strain energy density is defined as:

$$\Delta W_t = \oint \sigma d\varepsilon + \frac{{\sigma^2}_{max}}{2E} \quad (2)$$

Qualitatively Eq. (2) represents the summation of the area within the stabilized hysteresis loop (plastic component) and the elastic "unloading" energy from the tensile peak of the hysteresis loop (elastic component)[54], [60]. Previous work by Jahed et al. [54] suggested that for various forms of wrought magnesium from the AM, AZ and ZK families, one unique set of fitting constants C and m could be

utilized to predict the fatigue life in both uniaxial and multiaxial loading. Their study however did not include the AZ80 alloy or forged varieties of Mg. Fitting the fatigue data presented in Figure 10a with the generalized energy-life power relation in Eq. (1), a unique set of fitting constants were found for both the cast and wrought (extruded, CF and EF) varieties of AZ80 Mg presented in this study. The distinction is made between the cast and wrought forms in the implementation of this model as their microstructural attributes, texture and mechanical properties vary dramatically, and thus their cyclic characteristics should follow. Furthermore, Jahed suggested that various forms of wrought magnesium (extrusion, rolled sheet and rolled plate) can be characterized by the same unique set of fitting constants [54], similarly in this study, the data for the as-extruded and forged (CF and EF) material was grouped together and considered all to be of the "wrought" variety.

Utilizing these energy based models, the total strain energy density vs. number of cycles is presented in Figure 10 (a). For the as-cast samples, the results presented were from a combination of all orientations (LD,RD,TD) whereas the as-extruded is only from the extrusion direction. As previously mentioned, all of the forged material sample orientations were from the longitudinal direction of the forged billet. For all materials a subset of the results presented in Figure 8 which had strain measurement throughout the test were utilized for life modelling as it is required for calculation of the energy based parameters and life prediction for both models. For the CF and EF conditions, samples were taken from different regions within the cross section of the forging, as denoted next to each datapoint (once again corresponding with the locations denoted in Figure 2d).

Table 2 - Energy-based parameters for the JV and two parameter models for the as-cast, as-extruded, as well as closed die cast-forged and closed die extruded forged at 375 deg C and 20 mm/sec.

Material	JV Energy Based Model				Two Parameter Energy Based Model	
	E_e' (MJ/m^3)	E_f' (MJ/m^3)	B	C	C (MJ/m^3)	m
Cast [33]	3.5861	68.39	-0.309	-0.555	35.255	-0.467
Extruded	5.4468	634.19	-0.273	-0.962	40.478	-0.456
Cast-Forged	-					
Extruded-Forged						

As can be observed in Figure 10b, with regards to the as-cast material life prediction, almost all the life estimations fall within the bounds of a factor of 2.5, with almost equal numbers of data being under and over predicted. It can be observed that the cast-forged material has a larger amount of scatter amongst the data, which can be attributed to the aforementioned spatial variation in mechanical properties throughout the forging and the fact that the samples were taken from different locations throughout the same forging. For the cast-forged material, location 8 (as denoted by in both Figure 10a and b) is considered an outlier, as it has a significantly higher total strain energy density for a given life compared with all the other material varieties. This results in an expected conservative life prediction as both the JV and two parameter models overestimate the fatigue damage for this particular location within the forging. This overestimation is a direct result of the spatial variation in both texture and monotonic properties that can be observed in Figure 2 and Figure 4 respectively. More specifically, the web region (location 8) has a comparatively different texture and dramatically different strength and ductility in comparison to other regions within the forging like the flanges. This spatial variation in properties between the web and flanges is much less pronounced in the extruded-forged material albeit still marginally evident. Since the

web region of the cast-forged material has a considerably higher strength and ductility relative to the other locations in the forging for which the fitting constants are more representative of, the resulting life prediction is overly conservative at location 8 for the cast-forged material and lies well outside of the bounds of a factor of 2.5. Excluding this anomaly, the remainder of the life predictions using the two parameter model are quite reasonable and fall within the bounds of a factor of 2.5.

Figure 10c illustrates the fatigue life prediction for the as-received material (cast and extruded) for both of the models implemented here. It can be observed that for the as-cast material, both the two parameter and JV energy based models give very similar life estimates, which is to be expected since the fitting constants were generated specifically for cast material. However, it can be observed that the JV model gives a more accurate prediction for the as-extruded material as the two parameter model consistently predicts higher lives than "ideal". This can be attributed to the two parameter model being calibrated using data from all three forms of wrought material (extruded, CF and EF) which can be considered to be an accurate (albeit more approximate) approach.

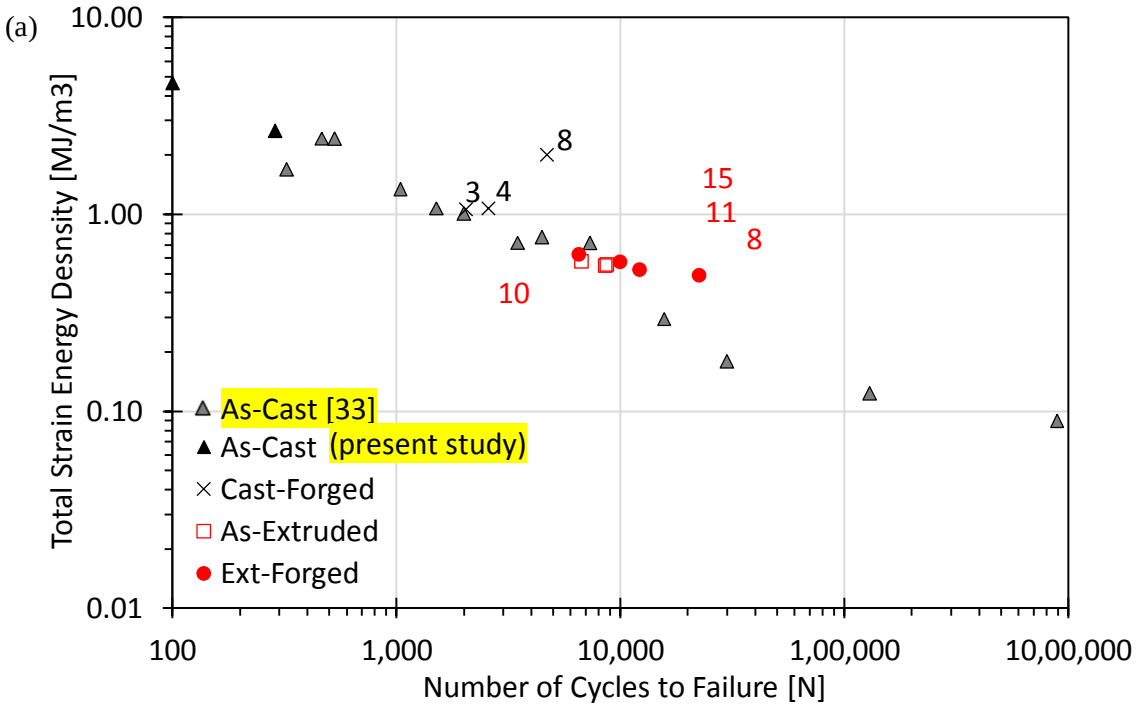

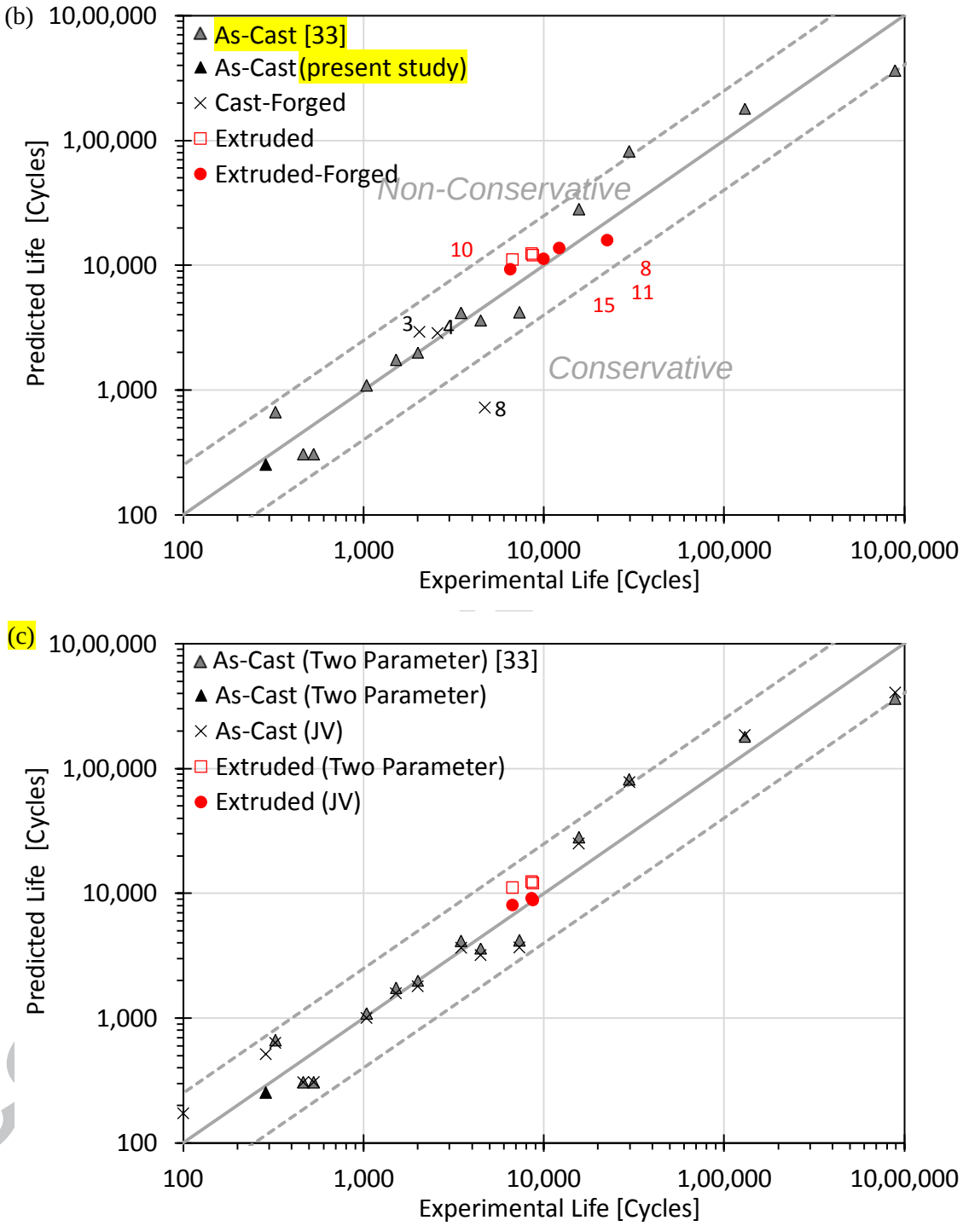

Figure 10- (a) JV damage parameter evolution with a number of cycles to failure for both as-received and forged AZ80 Mg; and (b) the correlation between two parameter predicted fatigue life and experimental life for both as-received and forged AZ80 Mg. (c) the correlation between prediction of two parameter and JV energy based model predictions for the as-received material. Locations within the billet for each forging are denoted beside each datapoint. The dashed lines in (b) and (c) denote bounds of ±2.5

4. Conclusions

Uniaxial quasi-static and fully-reversed fatigue experiments were conducted at various stress amplitudes, ranging from 140 – 190 MPa of as-cast, as extruded, cast-forged and extruded-forged AZ80 Mg alloy. The effects of various starting microstructure/texture and thermomechanical history on the quasi-static properties were investigated on a comparative basis. Based on the results the following conclusions can be drawn:

1. Following forging, both the cast-forged and extruded-forged material exhibited an increase in fatigue life in some instances of up to 15 times for a given stress amplitude. The degree of fatigue life improvement depending on the processing conditions and the type of base material.
2. All materials exhibited tension/compression asymmetry to varying degrees, depending on the thermomechanical processing conditions. It was discovered that the style of closed-die forging being investigated had spatially varying properties with texture orientations which varied based on the local forging directions and intensities which were dependent on the starting texture as well as the thermomechanical history.
3. The as-cast material possessed a random texture and exhibited diffuse extension twinning in the first reversal of cyclic testing at high-stress amplitudes. All of the textured materials cast-forged, extruded and extruded forged possessed sharp texture which resulted in extension twinning in compression during the second reversal at higher stress amplitudes.
4. Under fatigue testing, the materials all developed some form of mean strain, with the nature and magnitude of this mean strain being dependent on primarily its texture intensity and propensity to twin in either tension or compression reversals. The type of mean strain (tensile or compressive) depends upon both the orientation and intensity of the starting texture of the material.
5. The texture induced ratcheting and resulting mean strain evolution was most pronounced in the as-cast material and had a significant impact on the fatigue life.
6. Strain energy density was demonstrated to be a good parameter for predicting the fatigue damage for both cast and wrought forms of AZ80 Mg. Both a simple two parameter and more complex four parameter Jahed-Varvani energy based models were able to provide reliable life prediction for cast, extruded and closed-die forged AZ80 Mg at a variety of different stress amplitudes.

Acknowledgments

The financial support of the Natural Sciences and Engineering Research Council of Canada (NSERC) through the Automotive Partnership Canada (APC) under APCPJ 459269–13 grant with contributions from Multimatic Technical Centre, Ford Motor Company, and Centerline Windsor are acknowledged. The authors would also like to acknowledge J. McKinley from CanmetMATERIALS, Hamilton for forging trials.

References

[1] J. Pan, “Sound Package Design for Lightweight Vehicles,” *SAE Int.*, no. 10.4271/2015-01-2343, 2015.

[2] S. Begum, D. L. Chen, S. Xu, and A. A. Luo, “Low cycle fatigue properties of an extruded AZ31 magnesium alloy,” *Int. J. Fatigue*, vol. 31, no. 4, pp. 726–735, 2009.

[3] S. Hasegawa, Y. Tsuchida, H. Yano, and M. Matsui, “Evaluation of low cycle fatigue life in AZ31 magnesium alloy,” *Int. J. Fatigue*, vol. 29, no. 9–11, pp. 1839–1845, 2007.

[4] M. Lugo *et al.*, “Role of different material processing methods on the fatigue behavior of an AZ31 magnesium alloy,” *Int. J. Fatigue*, vol. 52, pp. 131–143, 2013.

[5] S. Hyuk Park, S. G. Hong, B. Ho Lee, W. Bang, and C. Soo Lee, “Low-cycle fatigue characteristics of rolled Mg-3Al-1Zn alloy,” *Int. J. Fatigue*, vol. 32, no. 11, pp. 1835–1842, 2010.

[6] F. Lv *et al.*, “Fatigue properties of rolled magnesium alloy (AZ31) sheet: Influence of specimen orientation,” *Int. J. Fatigue*, vol. 33,

no. 5, pp. 672–682, 2011.
[7] S. Ishihara, S. Taneguchi, H. Shibata, T. Goshima, and A. Saiki, "Anisotropy of the fatigue behavior of extruded and rolled magnesium alloys," *Int. J. Fatigue*, vol. 50, pp. 94–100, 2013.
[8] Q. Yu, J. Zhang, Y. Jiang, and Q. Li, "Multiaxial fatigue of extruded AZ61A magnesium alloy," *Int. J. Fatigue*, vol. 33, no. 3, pp. 437–447, 2011.
[9] H. Zenner and F. Renner, "Cyclic material behaviour of magnesium die castings and extrusions," *Int. J. Fatigue*, vol. 24, no. 12, pp. 1255–1260, 2002.
[10] R. Zeng, E. Han, and W. Ke, "A critical discussion on influence of loading frequency on fatigue crack propagation behavior for extruded Mg-Al-Zn alloys," *Int. J. Fatigue*, vol. 36, no. 1, pp. 40–46, 2012.
[11] Q. Guo, H. G. Yan, Z. H. Chen, and H. Zhang, "Fracture behaviors of AZ80 magnesium alloy during multiple forging processes," *Trans. Nonferrous Met. Soc. China (English Ed.*, vol. 16, no. 4, pp. 922–926, 2006.
[12] P. Moldovan, G. Popescu, D. Bojin, D. Constantinescu, and M. Pana, "Improving the fatigue resistance of magnesium alloys for forged parts in automotive industry," *Metal. Int.*, vol. 14, no. SPEC. ISS. 2, pp. 23–26, 2009.
[13] L. Wang *et al.*, "Effects of texture and grain size on mechanical properties of AZ80 magnesium alloys at lower temperatures," *Mater. Des.*, vol. 89, pp. 1–8, 2016.
[14] P. Moldovan and D. M. Constantinescu, "Magnesium Alloys for Automotive Applications," *Metal. Int.*, vol. 14, no. 7, pp. 19–23, 2009.
[15] J. Yoon and J. Lee, "Process design of Warm-Forging with extruded Mg-8Al-0.5Zn alloy for differential case in automobile transmission," *Int. J. Precis. Eng. Manuf.*, vol. 16, no. 4, pp. 841–846, 2015.
[16] M. Madaj, M. Greger, and V. Karas, "Magnesium-alloy die forgings for automotive applications," *Mater. Tehnol.*, vol. 49, no. 2, pp. 267–273, 2015.
[17] A. Gontarz and A. Dziubińska, "Forming of flat parts with ribs from magnesium alloy," *Aircr. Eng. Aerosp. Technol.*, vol. 86, no. 4, pp. 356–360, 2014.
[18] J. Yoon and S. Lee, "Warm forging of magnesium AZ80 alloy for the control arm in an automobile," *Proc. Inst. Mech. Eng. Part D J. Automob. Eng.*, vol. 229, no. 13, pp. 1732–1738, 2015.
[19] Q. Wang, Z. M. Zhang, X. Zhang, and J. M. Yu, "Precision forging technologies for magnesium alloy bracket and wheel," *Trans. Nonferrous Met. Soc. China (English Ed.*, vol. 18, no. SPEC. ISSUE 1, pp. s205–s208, 2008.
[20] V. Kevorkijan, "AZ80 and ZC71/SiC/12p closed die forgings for automotive applications: technical and economic assessment of possible mass production," *Materials science and technology*, vol. 19, no. 10. pp. 1386–1390, 2003.
[21] G. Kurz, B. Clauw, W. H. Sillekens, D. Letzig, and P. Manufacturing, "Die Forging of the Alloys Az80 and Zk60," *Mater. Soc. Annu. Meet.*, pp. 197–202, 2009.
[22] G. Rivers, "Cyclic Fatigue Testing of Wrought Magnesium AZ80 Alloy for Automotive Wheels," 2009.
[23] D. Kobold, T. Pepelnjak, G. Gantar, and K. Kuzman, "Analysis of deformation characteristics of magnesium AZ80 wrought alloy under hot conditions," *Stroj. Vestnik/Journal Mech. Eng.*, vol. 56, no. 12, pp. 823–832, 2010.
[24] H. T. Zhou, Q. B. Li, Z. K. Zhao, Z. C. Liu, S. F. Wen, and Q. D. Wang, "Hot workability characteristics of magnesium alloy AZ80-A study using processing map," *Mater. Sci. Eng. A*, vol. 527, no. 7–8, pp. 2022–2026, 2010.
[25] G. Z. Quan, T. Song, Y. J. Zhou, F. B. Wang, and J. Zhou, "Relationship between mechanical properties and grain size of AZ80 at 350 °c under different strain rates," *Trans. Nonferrous Met. Soc. China (English Ed.*, vol. 20, no. SUPPL. 2, pp. 0–4, 2010.
[26] G. Rivers, "Cyclic Fatigue Behaviour of Wrought AZ80 Magnesium Alloy from Forged Automotive Wheel," McMaster University, 2011.
[27] H. Z. Li, X. Y. Wei, J. Ouyang, J. Jiang, and Y. Li, "Hot deformation behavior of extruded AZ80 magnesium alloy," *Trans. Nonferrous Met. Soc. China (English Ed.*, vol. 23, no. 11, pp. 3180–3185, 2013.
[28] Z. Su, L. Wan, C. Sun, Y. Cai, and D. Yang, "Hot deformation behavior of AZ80 magnesium alloy towards optimization of its hot workability," *Mater. Charact.*, vol. 122, pp. 90–97, 2016.
[29] D. Toscano, S. K. Shaha, B. Behravesh, H. Jahed, and B. Williams, "Effect of forging on the low cycle fatigue behavior of cast AZ31B alloy," *Mater. Sci. Eng. A*, vol. 706, no. August, pp. 342–356, 2017.
[30] A. Gryguc, H. Jahed, B. Williams, and J. McKinley, "Magforge – Mechanical behaviour of forged AZ31B extruded magnesium in monotonic compression," *Mater. Sci. Forum*, vol. 828–829, pp. 291–297, 2015.
[31] A. Gryguc, S. K. Shaha, H. Jahed, M. Wells, B. Williams, and J. McKinley, "Tensile and fatigue behaviour of as-forged AZ31B extrusion," *Frat. ed Integrita Strutt.*, vol. 10, no. 38, pp. 251–258, 2016.
[32] A. Gryguc, S. K. Shaha, S. B. Behravesh, H. Jahed, M. Wells, and B. Williams, "Compression Behaviour of Semi-Closed Die Forged AZ80 Extrusion," *Charact. Miner. Met. Mater. 2017*, pp. 361–369, 2017.
[33] A. Gryguc *et al.*, "Monotonic and cyclic behaviour of cast and cast-forged AZ80 Mg," *Int. J. Fatigue*, vol. 104, 2017.
[34] S. M. H. Karparvarfard, S. K. Shaha, S. B. Behravesh, H. Jahed, and B. W. Williams, "Microstructure, texture and mechanical behavior characterization of hot forged cast ZK60 magnesium alloy," *J. Mater. Sci. Technol.*, vol. 33, no. 9, pp. 907–918, 2017.
[35] D. Toscano, S. K. Shaha, B. Behravesh, H. Jahed, and B. Williams, "Effect of Forging on Microstructure, Texture, and Uniaxial Properties of Cast AZ31B Alloy," *J. Mater. Eng. Perform.*, vol. 26, no. 7, pp. 3090–3103, 2017.
[36] H. He, S. Huang, Y. Yi, and W. Guo, "Simulation and experimental research on isothermal forging with semi-closed die and multi-stage-change speed of large AZ80 magnesium alloy support beam," *J. Mater. Process. Technol.*, vol. 246, pp. 198–204, 2017.
[37] Z. Wang, Y. Yang, B. Li, Y. Zhang, and Z. Zhang, "Effect of hot-deformation on microstructure and mechanical properties of AZ80 magnesium alloy," *Mater. Sci. Eng. A*, vol. 582, pp. 36–40, 2013.
[38] A. A. Roostaei and H. Jahed, "Role of loading direction on cyclic behaviour characteristics of AM30 extrusion and its fatigue damage modelling," *Mater. Sci. Eng. A*, vol. 670, pp. 26–40, 2016.
[39] G. Yu, "Forging Specimen Design for Magnesium Alloys," 2016.
[40] F. Nový, M. Janeček, V. Škorik, J. Muller, and L. Wagner, "Very high cycle fatigue behaviour of as-extruded AZ31, AZ80, and ZK60 magnesium alloys," *Int. J. Mater. Res.*, vol. 100, no. 3, pp. 288–291, 2009.
[41] D. Sarker and D. L. Chen, "Texture transformation in an extruded magnesium alloy under pressure," *Mater. Sci. Eng. A*, vol. 582, pp. 63–67, 2013.
[42] J. Albinmousa and H. Jahed, "Multiaxial effects on LCF behaviour and fatigue failure of AZ31B magnesium extrusion," *Int. J. Fatigue*, vol. 67, pp. 103–116, 2014.
[43] S. Dong *et al.*, "Characteristic cyclic plastic deformation in ZK60 magnesium alloy," *Int. J. Plast.*, vol. 91, pp. 25–47, 2017.

[44] X. M. Chen, Y. C. Lin, and J. Chen, "Low-cycle fatigue behaviors of hot-rolled AZ91 magnesium alloy under asymmetrical stress-controlled cyclic loadings," *J. Alloys Compd.*, vol. 579, pp. 540–548, 2013.
[45] C. A. Sager *et al.*, "PHYSICAL METALLURGY OF Mg AZ80 ALLOYS FOR FORGING APPLICATIONS," *Mater. Soc. Annu. Meet.*, vol. 12, no. April, pp. 405–410, 2009.
[46] Y. Ogushi, E. Mostaed, D. Dellasega, M. Vedani, H. Miyamoto, and H. Fujiwara, "Aging behavior of ECAP processed AZ80 Mg alloy," *IOP Conf. Ser. Mater. Sci. Eng.*, vol. 63, no. 1, 2014.
[47] H. Yu, S. Hyuk, and B. S. You, "Development of extraordinary high-strength Mg – 8Al – 0 . 5Zn alloy via a low temperature and slow speed extrusion," *Mater. Sci. Eng. A*, vol. 610, pp. 445–449, 2014.
[48] Y. Cai *et al.*, "Hot deformation characteristics of AZ80 magnesium alloy: Work hardening effect and processing parameter sensitivities," *Mater. Sci. Eng. A*, vol. 687, no. December 2016, pp. 113–122, 2017.
[49] E. Kalatehmollaei, H. Mahmoudi-Asl, and H. Jahed, "An asymmetric elastic-plastic analysis of the load-controlled rotating bending test and its application in the fatigue life estimation of wrought magnesium AZ31B," *Int. J. Fatigue*, vol. 64, pp. 33–41, 2014.
[50] Y. Xiong and Y. Jiang, "Cyclic deformation and fatigue of rolled AZ80 magnesium alloy along different material orientations," *Mater. Sci. Eng. A*, vol. 667, pp. 58–67, 2016.
[51] R. Zhu, W. Ji, Y. Wu, X. Cai, and Y. Yu, "Effect of aging treatment on low-cycle fatigue behavior of extruded Mg-8Al-0.5Zn alloys," *Mater. Des.*, vol. 41, pp. 203–207, 2012.
[52] Y. C. Lin, Z. H. Liu, X. M. Chen, and J. Chen, "Stress-based fatigue life prediction models for AZ31B magnesium alloy under single-step and multi-step asymmetric stress-controlled cyclic loadings," *Comput. Mater. Sci.*, vol. 73, pp. 128–138, 2013.
[53] A. Gryguc, S.B. Behravesh, S.K. Shaha, H. Jahed, M. Wells, B. Williams, X. Su, "Effect of warm forging on monotonic and cyclic behaviour of AZ80 casting," *Int. J. Fatigue*, no. SI: Proceedings of FDSM XI, 2017.
[54] H. Jahed and J. Albinmousa, "Multiaxial behaviour of wrought magnesium alloys - A review and suitability of energy-based fatigue life model," *Theor. Appl. Fract. Mech.*, vol. 73, pp. 97–108, 2014.
[55] F. Ellyin, K. Golos, and Z. Xia, "In-Phase and Out-of-Phase Multiaxial Fatigue," *J. Eng. Mater. Technol.*, vol. 113, no. 1, p. 112, 1991.
[56] H. Jahed and A. Varvani-Farahani, "Upper and lower fatigue life limits model using energy-based fatigue properties," *Int. J. Fatigue*, vol. 28, no. 5–6, pp. 467–473, 2006.
[57] S. H. Park, S. G. Hong, W. Bang, and C. S. Lee, "Effect of anisotropy on the low-cycle fatigue behavior of rolled AZ31 magnesium alloy," *Mater. Sci. Eng. A*, vol. 527, no. 3, pp. 417–423, 2010.
[58] J. Albinmousa, H. Jahed, and S. Lambert, "An Energy-Based Fatigue Model for Wrought Magnesium Alloy under Multiaxial Load," *Ninth Int. Conf. Multiaxial Fatigue Fract.*, pp. 471–478, 2010.
[59] A. A. Roostaei and H. Jahed, "Multiaxial cyclic behaviour and fatigue modelling of AM30 Mg alloy extrusion," *Int. J. Fatigue*, vol. 97, pp. 150–161, 2017.
[60] S. M. H. Karparvarfard, S.K.Shaha, S. B. Behravesh, H. Jahed, and B. W. Williams, "Fatigue Characteristics and modeling of Cast and Cast-Forged ZK60 Magnesium Alloy," *Int. J. Fatigue*, no. November 2017, 2018.